On the use of a modified optical flow algorithm for the correction of axial strain estimates in ultrasonic elastography for medical diagnosis

A. Lorenz[1] , G. Schäpers[1], H.-J. Sommerfeld[2], M. Garcia-Schürmann[2], S. Philippou[3], T. Senge[2], H. Ermert[1]

[1]Ruhr-Universität Bochum, Institut für Hochfrequenztechnik, 44780 Bochum
[2]Ruhr-Universität Bochum, Urologische Klinik, 44627 Herne
[3]Ruhr-Universität Bochum, Abteilung für Pathologie, 44781 Bochum

Summary: We present a new system for imaging the elastic properties of prostate tissue *in vivo* by estimating, correcting, and visualizing the tissue strain from local axial time shift estimates. We show that the image quality of the strain images can be significantly improved by the correction of lateral motion components using a modified optical flow algorithm. Phantom images and clinical in vivo data are presented which show the high potential of the system for early tumor detection.

INTRODUCTION

Tumors of the prostate exhibit a significant mechanical hardness in comparison to the surrounding tissue. However, they often cannot be reliably detected in the B-mode image. For this reason digital palpation of the prostate is still a major tool in tumor diagnostics. Ultrasonic elastography estimates the tissue elasticity from an image series recorded under varying axial tissue compression usually applied by the transducer itself. As a new imaging modality elastography promises to significantly support conventional prostate screening methods.

The tissue elasticity is estimated within a region of interest from the axial tissue motion whose derivative is the tissue strain. Elastography was first described in (1) and a significant improvement for the calculation of the axial time shifts was introduced in (2). The signal-to-noise-ratio of the strain images (SSNR) can be significantly improved by averaging several images (3). Assuming constant stress throughout the imaging plane the visualized strain is proportional to the Young's modulus of the material. We show in this paper that imaging of the tissue strain provides important information about the elasticity of the examined organ. We present results from a clinical in vivo study of the human prostate.

In order to obtain an estimate for the axial strain two corresponding windowed A-lines are numerically compared by cross-correlation techniques which are applied segmentwise to the acquired rf-data under the assumption of a uniform axial compression of the tissue. However clinical in vivo data suffer from significant lateral motion which deteriorates the phase sensitive axial motion estimates.

To correct for lateral motion artifacts a new method is presented which uses the global two-dimensional motion field of the demodulated rf-data to correct the complex baseband signals prior to the axial time shift estimation using the method described in (2). The calculation of the two-dimensional motion field is performed by a modified "optical flow" algorithm described in the next section. The motion vectors are used to correct the

corresponding A-lines according to the encountered lateral deformation. We show that this method is able to improve the strain estimates significantly especially on data with low signal-to-noise conditions.

METHODS

The two-dimensional tissue motion is estimated by an algorithm presented in (4), which uses the following "optical flow" equation:

$$\frac{dI}{dt} = \frac{\partial I}{\partial x}\frac{dx}{dt} + \frac{\partial I}{\partial y}\frac{dy}{dt} + \frac{\partial I}{\partial t} = 0 \tag{1}$$

Equation (1) expresses the fact that there is no change of image brightness I as a function of space (x,y) and time t of a certain pixel during the tissue motion. Introducing $I_x = \partial I / \partial x$, $I_y = \partial I / \partial y$, $I_t = \partial I / \partial t$ and $\partial x / \partial t = u$, $\partial y / \partial t = v$, the motion vector $\vec{v}(P_i) = (u\ v)^T$ can be estimated from the pixel intensities in the neighborhood $\Omega(P_i)$ of location P_i using the following least-squares formulation (4):

$$\sum_{P(x,y)\in\Omega(P_i)} W^2(P_i,x,y)(I_x u + I_y v + I_t)^2 \xrightarrow{(u,v)} \min \tag{2}$$

The derivatives $\nabla I = (I_x, I_y)^T$ and I_t are estimated from finite differences around P_i. $W(P_i,x,y)$ is a Gaussian shaped weighting function which reduces the influence of points with increasing distance from P_i. We use a sector shaped area $\Omega(P_i) = \Omega_x \times \Omega_y$ centered around P_i with lengths $\Omega_x = 5.4°$ and $\Omega_y = 2$ mm. Equation (2) can be rewritten as

$$\mathbf{A}^T W^2 \mathbf{A} \cdot \vec{v} + \mathbf{A}^T W^2 \cdot \vec{b} = 0 \text{ with } \mathbf{A} = [\nabla I(P_1), \nabla I(P_2),...,\nabla I(P_N)]^T, \tag{3}$$

$$\text{and } \vec{b} = [I_t(P_1), I_t(P_2),...I_t(P_N)]^T \ \forall \ P_j \in \Omega(P_i)$$

and a solution of Equation (3) can be obtained by a singular value decomposition (SVD).

To use the full scope of the optical flow algorithm the ground motion is calculated and subtracted by a simple cross-correlation search (5) which is applied at the center of the image prior to the motion estimation (Equation (4)). The motion vector (m,n) corresponding to the maximum cross-correlation coefficient $\rho_{m,n}$ in the search region is subtracted from the image data by moving the area of interest before applying the optical flow algorithm.

$$\rho_{m,n} = \frac{\sum_{i=1}^{l}\sum_{j=1}^{k}(X_{i,j} - \overline{X})(Y_{i+m,j+n} - \overline{Y})}{\sqrt{\sum_{i=1}^{l}\sum_{j=1}^{k}(X_{i,j} - \overline{X})^2 (Y_{i+m,j+n} - \overline{Y})^2}} \xrightarrow{(m,n)} \max,\ m < m_{\max},\ n < n_{\max} \tag{4}$$

For higher accuracy the search was performed iteratively by subtracting the calculated motion vector from the image data after each cycle of the iteration. The iteration was stopped (usually within 1-3 iterations) when the new calculated motion vector was close or lower than the derivation length of the finite differences.

The lateral motion component of the calculated motion field was used to interpolate the baseband data of the first image of the image pair linearly between the two nearest A-lines:

$$x'_{ib}(t_n) = \begin{cases} \vdots & \vdots \\ (1 - u_i(t_n))x_{ib}(t_n) + u_i(t_n)x_{i-1b}(t_n) & \text{für} \quad 0 \leq u_i(t_n) \leq 1 \\ (1 - u_i(t_n) - 1)x_{i-1b}(t_n) + (u_i(t_n) - 1)x_{i-2b}(t_n) & \text{für} \quad 1 \leq u_i(t_n) \leq 2 \\ \vdots & \vdots \end{cases} \tag{5}$$

The index i describes the A-line location, and x_{ib} refers to the baseband data. t_n describes discrete sampling positions in the axial direction and u_i refers to the lateral motion components obtained with the above modified estimator.

Our system used for data acquisition is described in (6). We acquired elastographic image sequences using a transrectal probe with sector scan geometry. The sequences contained of 10 images which were processed as explained above. In addition we obtained a volume data set of B-mode images of the whole gland. All patients of this study had a clinical indication for radical prostatectomy. Therefore several histological specimens were available at different positions within the gland. From this data base corresponding triples consisting of a B-mode image, a histology image, and an elastography sequence, were selected by the physicians.

RESULTS

FIGURE 1 describes the influence of the lateral motion correction on the signal-to-noise ratio of the strain images (SSNR). FIGURE 1a shows the motion vector field of the whole sequence indicating strong lateral motion on the left half of the image (r = range, Θ = azimuth). FIGURE 1b shows the SSNR before and after correction yielding a significant improvement in areas with large lateral motion components. FIGURE 1c shows the SSNR improvement obtained by averaging. Combining both methods can significantly improve the image quality; in some regions we obtain up to 10 dB improvement of the SSNR.
FIGURE 2 shows images obtained from a sponge phantom. At the center of the image there is an agar-agar cylinder which cannot be seen in the B-mode image. The cylinder is approximately 4 times harder than the surrounding material.
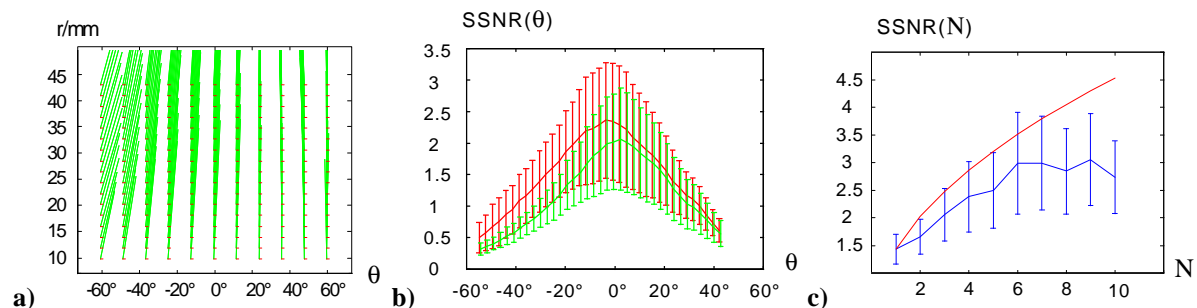

FIGURE 1: a) Cumulated motion over a sequence of 10 images of a homogeneous sponge phantom (r = range, Θ = azimuth. **b)** SNR of a single strain image before (lower curve) and after correction of lateral motion (upper curve). The errorbars indicate one standard deviation obtained over the sequence of 10 images. **c)** Improvement of SNR with increasing number of compounded images.
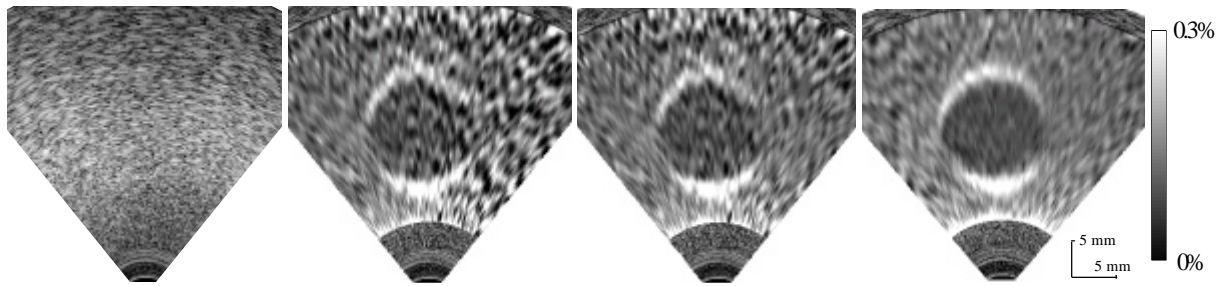
FIGURE 2: Sponge phantom with hard inclusion which is not visible in the B-mode image. **a)** B-mode image. **b)** Strain image without correction. **c)** Strain image with lateral correction. **d)** Strain image with lateral correction and averaging

The strain images show the typical axial strain pattern of a hard inclusion in a soft background. Lateral motion artifacts on the right half of the image were corrected by our algorithm and additional averaging could further improve the image quality. All images are displayed over the same dynamic range.

FIGURE 3 presents images obtained from a voluntary patient with prostate carcinoma which shows the potential of elastography for early tumor detection. The tumor cannot be seen in the B-mode image, however in the elastogram there is a distinct hard area. The location of the tumor was marked by a pathologist. In addition to the hard tumor area several other hard inclusions can be seen in the images which mostly result from stones.
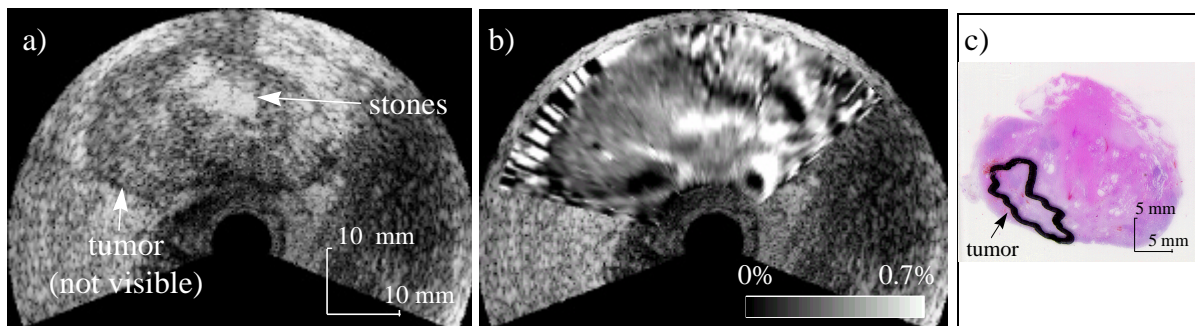

FIGURE 3: Patient with prostate carcinoma which was not visible in the B-mode image. **a)** B-mode image. **b)** *in vivo* strain image. **c)** histological specimen marked by a pathologist

REFERENCES

1. Ophir J., Céspedes I., Ponnekanti H., Yazdi Y., Li X., "Elastography: a quantitative method for imaging the elasticity of biological tissues," *Ultrason. Imag.*, vol. 13, pp. 111-114, 1991.
2. Pesavento A., Perrey C., Krueger M., Ermert H., "A time-efficient and accurate strain estimation concept for ultrasonic elastography using iterative phase zero estimation," submitted to *IEEE Trans. Ultrason., Ferroelect., Freq. Control*, 1998.
3. Varghese T., Ophir J., "Performance optimization in elastography: multicompression with temporal stretching," *Ultrason. Imag.*, vol. 18, pp. 193-214, 1996
4. Lucas B. D., Kanade T., "An iterative image registration technique with an application to stereo vision," *Proc. DARPA Image Understanding Workshop*, pp. 121-130, 1981.
5. Trahey G. E., Hubbard S. M., von Ramm O. T., "Angle dependent ultrasonic blood flow by frame-to-frame correlation of B-mode images," *Ultras.*, vol. 26, pp. 271-276, 1988.
6. Lorenz A., Sommerfeld H.-J., Schürmann M. G., Philippou S., Senge T., and Ermert H., "Diagnosis of prostate carcinoma using multicompression strain imaging: data acquisition and first in vivo results," *Proc. of the IEEE 1998 Ultrasonic Symposium*, to be published, 1998.